Supplementary Information

Deep reconstruction of crystalline-amorphous heterojunction electrocatalysts for efficient and stable water and methanol electrolysis

*Fang Zheng[a], Mayur A. Gaikwad[a], Zhenhua Fang[a], Suyoung Jang[a], Jin Hyeok Kim[a]**

[a] Optoelectronics Convergence Research Center and Department of Materials Science and Engineering, Chonnam National University, Yongbong-Dong, Buk-Gu, Gwangju 61186, South Korea

Corresponding author E-mail address: jinhyeok@chonnam.ac.kr

1. Experimental section

1.1 Chemicals

Nickel foam (NF), cobalt nitrate ($Co(NO_3)_2·6H_2O$), iron nitrate ($Fe(NO_3)_3·9H_2O$), 2-methylimidazole ($C_4H_6N_2$), and thioacetamide (C_2H_5NS), ruthenium(IV) oxide (RuO_2), activation carbon, and N-Methyl Pyrrolidone (C_5H_9NO) were purchased form Sigma-Aldrich. All reagents did not require further purification. NF was used as a substrate, which was ultrasonically cleaned with ethanol and deionized water for 5 min, respectively.

1.2 Synthesis of ZIF-67

Firstly, $Co(NO_3)_2·6H_2O$ (0.5 mmol, 0.1455 g) was dissolved into 10 mL Milli Q distilled water (DI water) and then NF (4 × 1 cm^2) immersed into solution 30 min. Then, $C_4H_6N_2$ (4 mmol, 0.3284 g) was dissolved into 10 mL DI water and then quickly added into the above solution and kept for 2 h. Thus, ZIF-67 can be received after washing with distilled water and dried 12 h at 60 ℃.

1.3 Synthesis of Co-Ni_3S_2 and Ni_3S_2

Synthesis of Co-Ni_3S_2 by solvothermal method using ZIF-67 as Co source. First, 0.6 g C_2H_5NS was dissolved in 60 mL ethanol and kept stirring for 10 min. Then, a piece of ZIF-67 on the NF was immersed in the above solution, and solvothermal process was performed at 120 °C for 4 h. After that, Co-Ni_3S_2 was prepared by washing with water and drying at 50 °C. To verify that NF also participated in the reaction as a nickel source, only pure NF was added to prepare pure Ni_3S_2 through the above method.

1.4 Synthesis of FeBO/Co-Ni_3S_2

FeBO/Co-Ni_3S_2 heterostructure was prepared by using Co-Ni_3S_2 as the substrate to support FeBO. First, the NF loaded with Co-Ni_3S_2 was placed in 47.5 ml of deionized water solution containing 0.5 mmol $Fe(NO_3)_3 \cdot 9H_2O$. Subsequently, 2.5 ml of $NaBH_4$ solution (0.5M) was gradually added to the above solution. After reacting at room temperature for 2 h, wash with plenty of water. The final product was dried at 50 °C overnight for further characterization and catalytic activity analysis. For comparison, NF-loaded FeBO nanostructures were also prepared in the same way. The electrocatalyst loading was calculated by weighing the NF electrode before and after catalyst synthesis. In this work, the electrocatalyst loading of FeBO/Co-Ni_3S_2 was approximately 3.8 mg cm^{-2}.

1.5 Preparation of RuO_2 electrode

RuO_2 was coated on the NF to prepare RuO_2 catalyst by universal approach. A total 6 mg RuO_2 was ultrasonically dispersed for at least 5 min in a mixture solution containing 0.16 mL of NMP and PVDP, and 1 mg Activation carbon.

1.6 Characterizations

Powder X-ray diffraction (XRD) was carried out on a X'Pert PRO Multi-Purpose X-Ray Diffractometer (PANalytical) using Cu Kα radiation. Raman spectra were studied by NRS-5100 using 532 nm laser source. Fourier transform infrared (FT-IR) were collected on a Spectrum 400. The morphology and microstructure of the prepared materials were tested by field emission scanning electron microscope (FE-SEM Gemini 500 + EDS (Oxford)) and field emission transmission electron microscope (FE-TEM, JEM-2100F, JEOL LTD). High-performance X-ray photoelectron spectroscopy (HP-XPS, K-ALPHA+) was used to characterize the elemental

information of catalysts. The electro-oxidation of methanol to formate was confirmed using ^{1}H NMR (400 MHz) AVANCE III HD 400.

1.7 Electrochemical measurement

The electrochemical performance was tested at an Autolab potentiostat (CHI Instruments, USA) using a three-electrode system. Platinum electrode and Ag/AgCl electrode were used as counter electrode and reference electrode, respectively, and the as-prepared materials on NF were used as working electrode. For electrocatalytic reactions, 1 M KOH and 1 M KOH + 0.5 M methanol were employed as the electrolytes, respectively. All the electrochemical experiments were carried out in electrolyte at 25 ℃. The area of the work electrode immersed in the electrolyte is 1 × 1 cm^2. Linear sweep voltammetry (LSV) was tested at scan rate of 1 mV s^{-1}. Convert the potential measured in this work to a reversible hydrogen electrode (RHE) according to equation E (*vs.* RHE) = E (*vs.* Ag/AgCl) + 0.197 + 0.059 × pH. The overpotential (η) was calculated according to the following equation: η = E (*vs.* RHE) – 1.23 V. Electrochemical impedance spectroscopic (EIS) was carried out using a high-performance potentiostat (Zive Potentiostat/Galvanostat/EIS, Wonatech, Republic of Korea) at a bias potential of 300 mV in the frequency range of 0.1 Hz-10000 Hz. Electrochemical active surface areas (ECSAs) were calculated based on the formula: ECSAs = C_{dl}/C_s. Among them, the double-layer capacitance (C_{dl}) was obtained by cyclic voltammetry (CV), while for Ni-/Co-based catalysts, C_s is usually adopted at 0.04 mF cm^{-2}. CV was tested in non-Faradaic region at scan rates of 20 to 100 mV s^{-1}. The prepared electrocatalysts' long-term stability was tested using chronopotentiometry (CP) at a current density of 10 mA cm^{-2} and a measurement time of 100 or 25 h. The overall water and methanol splitting uses FeBO/Co-Ni_3S_2 as anode and cathode.

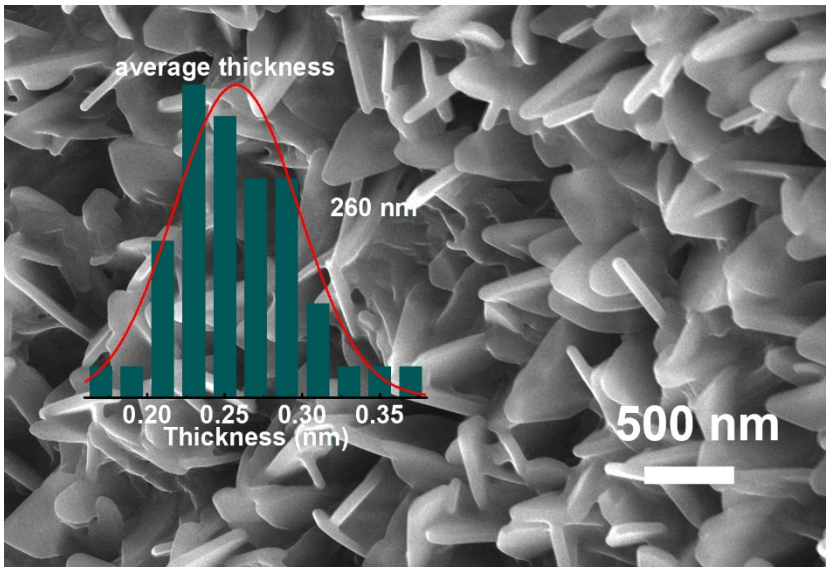

Fig. S1. FT-SEM image of ZIF-67.

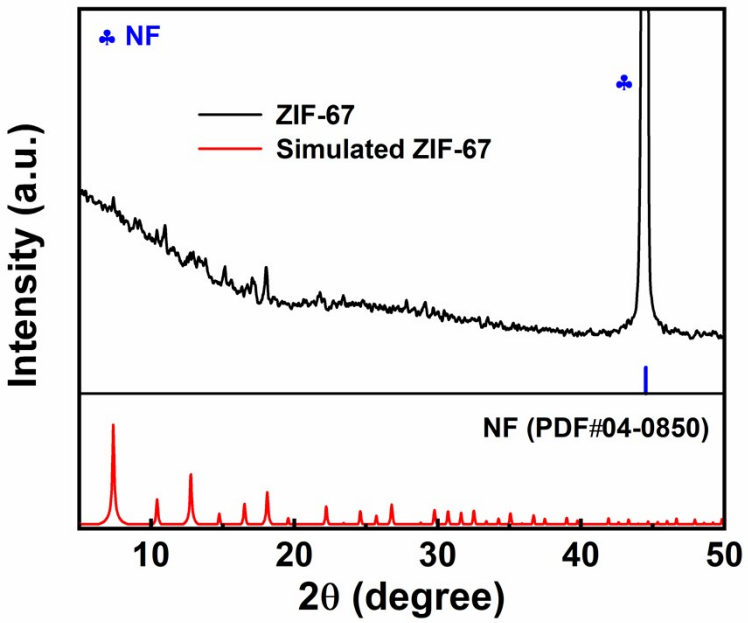

Fig. S2. XRD patterns of ZIF-67.

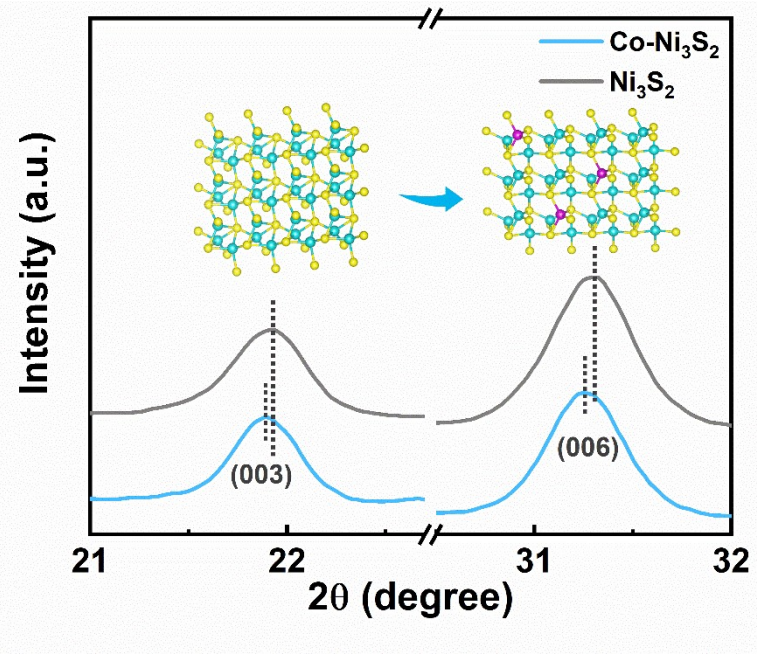

Fig. S3. Enlargement of partial XRD patterns of Co-Ni_3S_2 and Ni_3S_2.

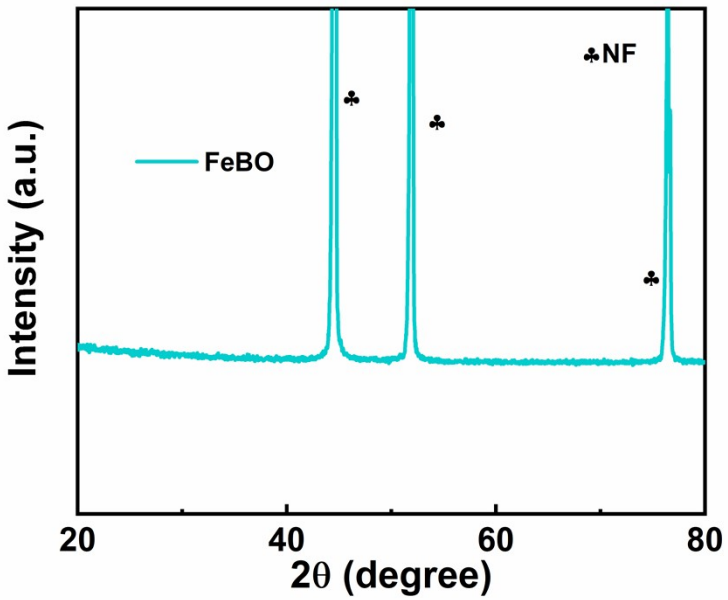

Fig. S4. XRD pattern of FeBO.

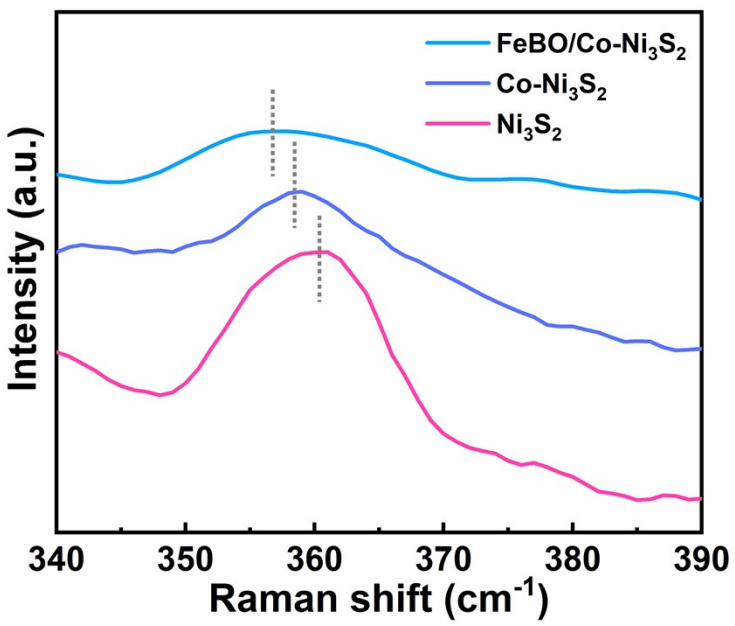

Fig. S5. Raman magnified image of FeBO/Co-Ni_3S_2, Co-Ni_3S_2, and Ni_3S_2 samples.

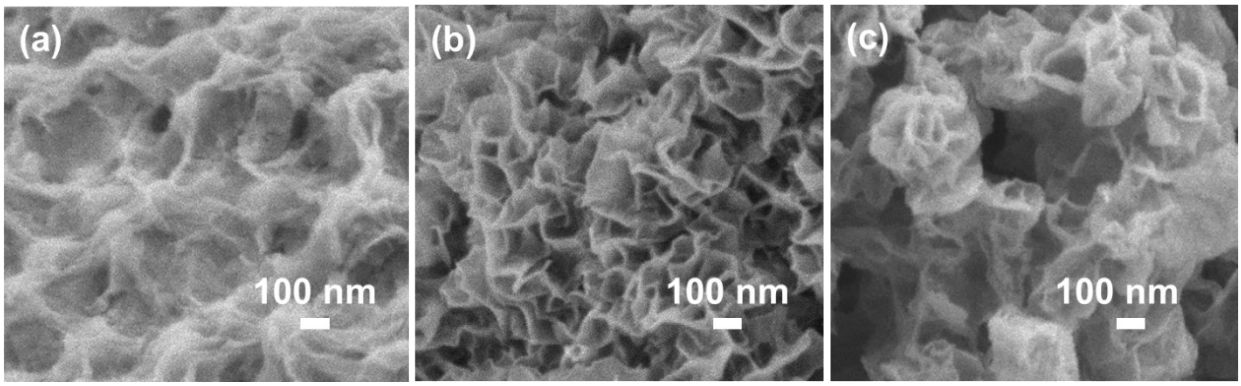

Fig. S6. FE-SEM images of (a) Ni_3S_2, (b) Co-Ni_3S_2, and (c) FeBO/Co-Ni_3S_2.

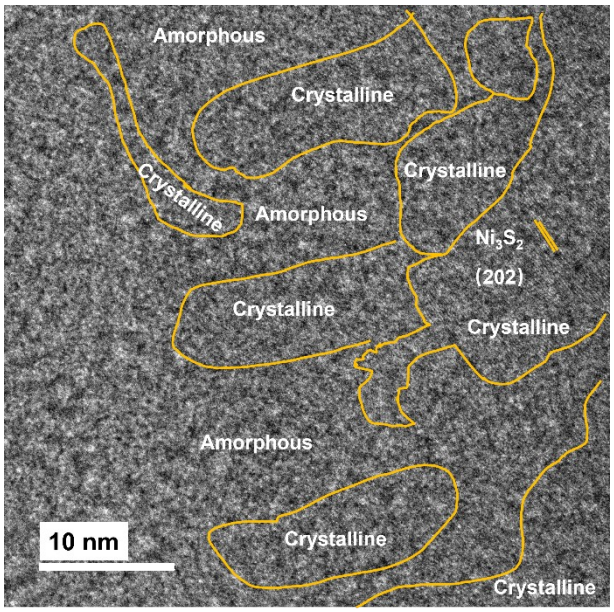

Fig. S7. HR-TEM image: the interfaces between crystalline Co-Ni_3S_2 and amorphous FeBO are marked with the yellow lines.

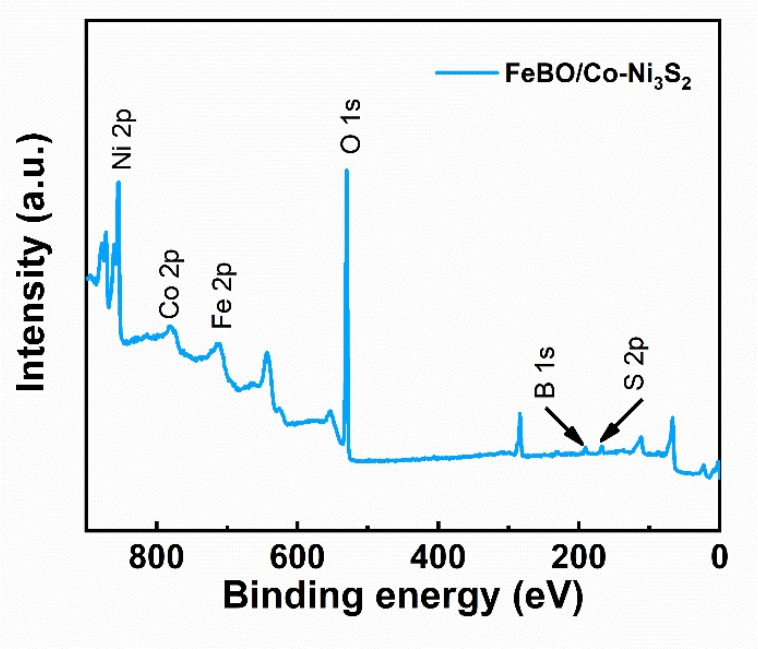

Fig. S8. XPS survey spectra of FeBO/Co-Ni_3S_2.

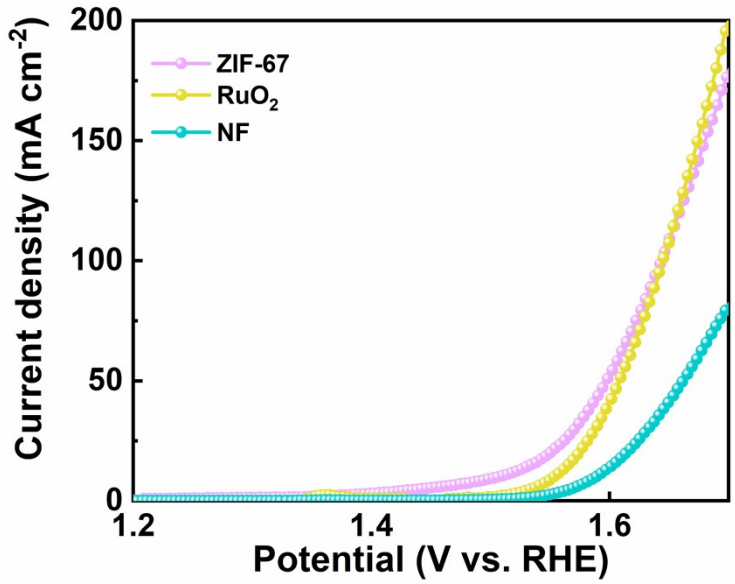

Fig. S9. LSV curves of ZIF-67, RuO_2 and NF for OER.

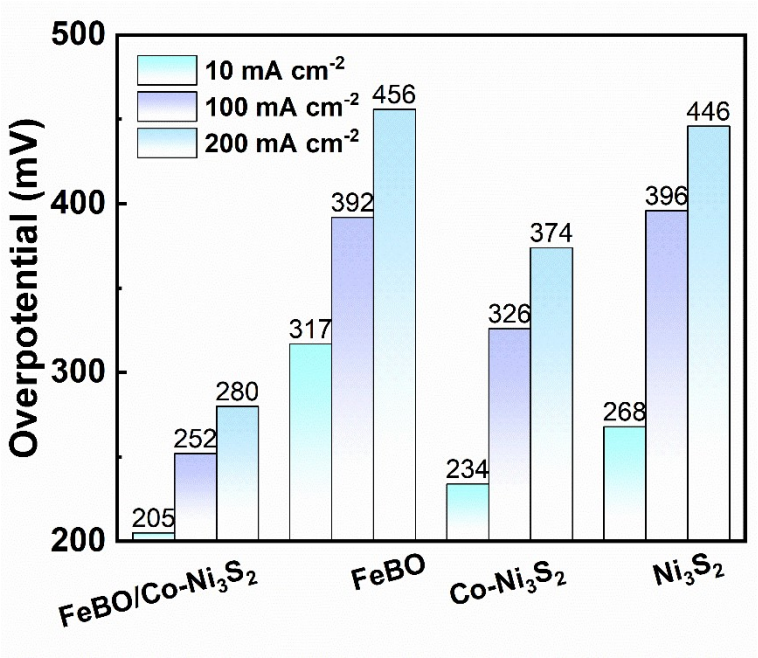

Fig. S10. Corresponding overpotentials of FeBO/Co-Ni_3S_2, FeBO, Co-Ni_3S_2, and Ni_3S_2 samples at different current densities.

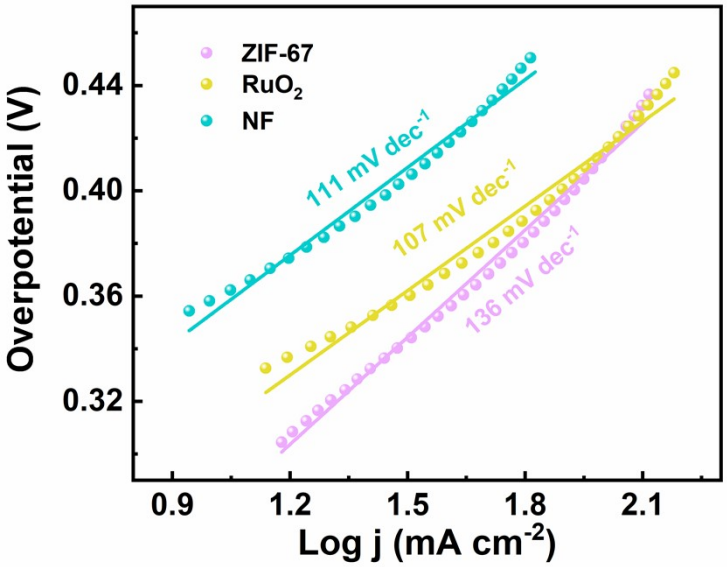

Fig. S11. Tafel slopes of ZIF-67, RuO_2, and NF.

Table S1. Comparison of OER performance between FeBO/Co-Ni_3S_2 and previously reported electrocatalysts using 1 M KOH as the electrolyte and NF as the substrate.

Catalyst	**Overpotential** (mV) @ j ($mAcm^{-2}$)	**Tafel slope** ($mV.dec^{-1}$)	**Stability (h)** @ j ($mAcm^{-2}$)	**Ref**
FeBO/Co-Ni_3S_2	**205 (η_{10})** **253 (η_{100})**	**42**	**100** (η_{10})	**This work**
Fe-Ni_3S_2/NF	214 (η_{10})	54	20 (η_{10})	[1]
MoS_2/Ni_3S_2 heterostructures	218 (η_{10})	76	10 (η_{10})	[2]
MoS_2–Ni_3S_2 HNRs/NF	249 (η_{10})	57	48 (η_{40})	[3]
Ni_2P-Ni_3S_2 HNAs/NF	210 (η_{10})	62	24 (η_{10})	[4]
Au/Ni_3S_2/NF	230 (η_{10})	51	60 (η_{10})	[5]
NiMoS	260 (η_{10})	59	15 (η_{120})	[6]
f-NiFe-LDH-B	209 (η_{10})	43.5	60 (η_{10})	[7]
NiFeB@OCC	255 (η_{20})	65	24 (η_{100})	[8]
Fe-doped Ni_3S_2/rGO@NF	247 (η_{20})	63	20 (η_{20})	[9]

Table S2. Values of R_s and R_{ct} in the samples for OER.

Sample	**R_s (Ω)**	**R_{ct} (Ω)**
FeBO/Co-Ni_3S_2	0.305	0.108
FeBO	0.283	163
Co-Ni_3S_2	0.302	1.14
Ni_3S_2	0.477	20.3

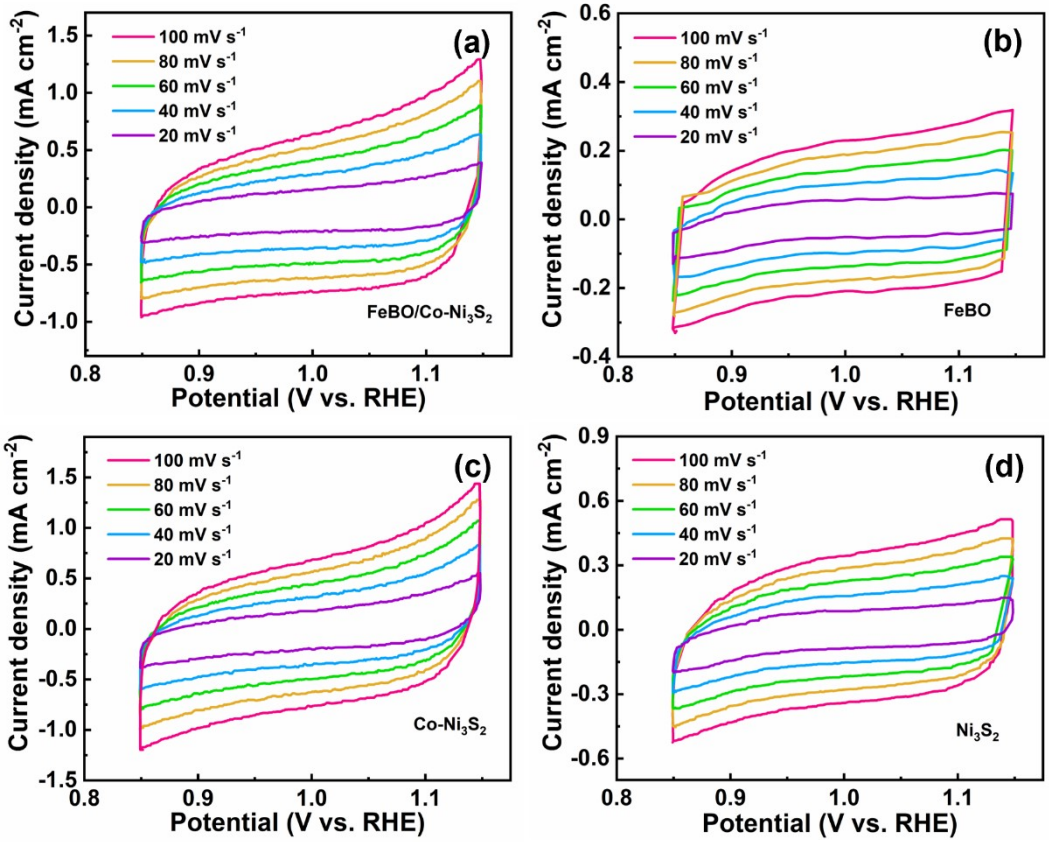

Fig. S12. The CV curves of (a) FeBO/Co-Ni_3S_2, (b) FeBO, (c) Co-Ni_3S_2, and (d) Ni_3S_2. All the curves were tested at different scan rates: 20, 40, 60, 80 and 100 mV s^{-1}.

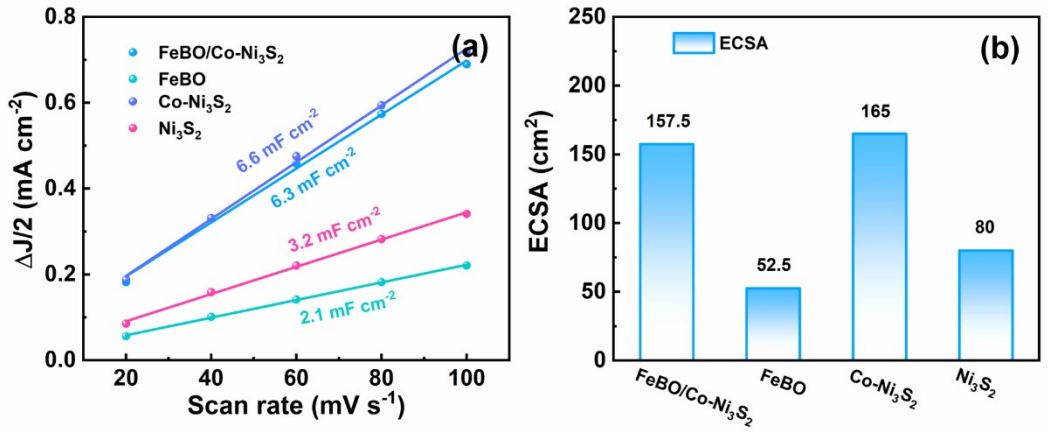

Fig. S13. The C_{dl} and ECSA values of the samples.

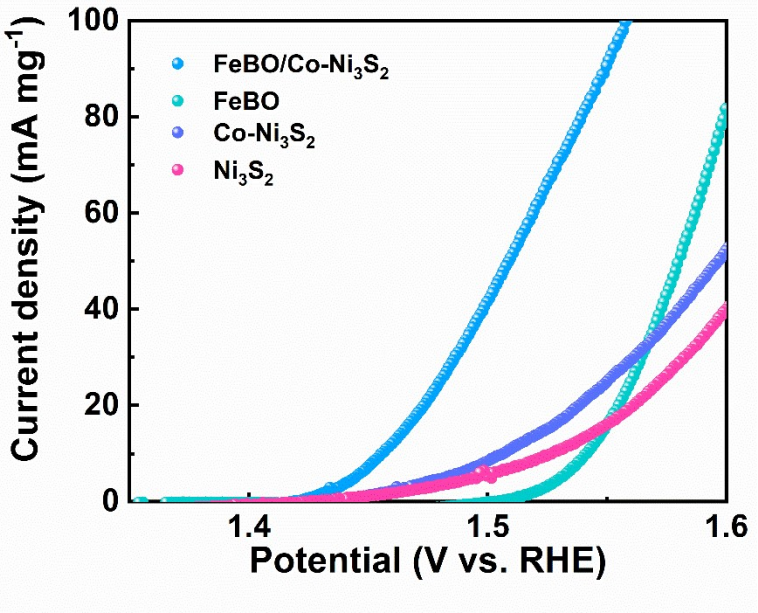

Fig. S14. The LSV curves normalized by mass.

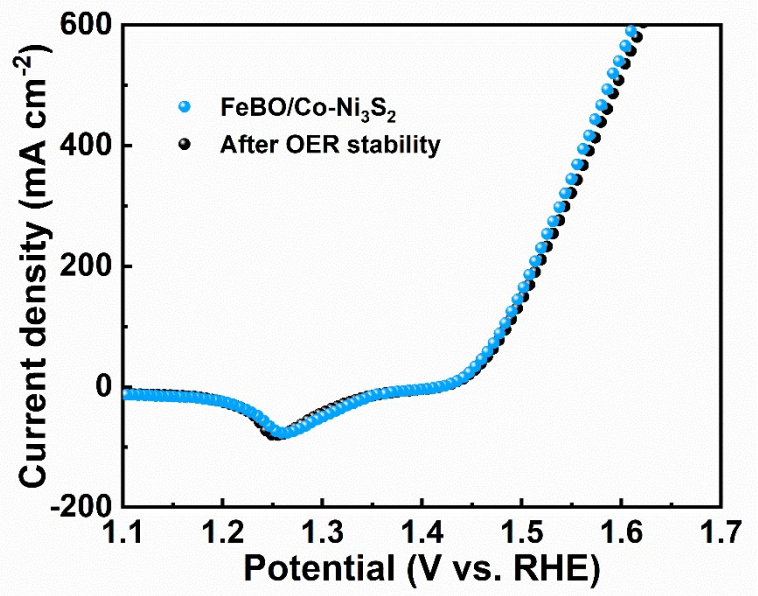

Fig. S15. The LSV curves before and after long-term stability.

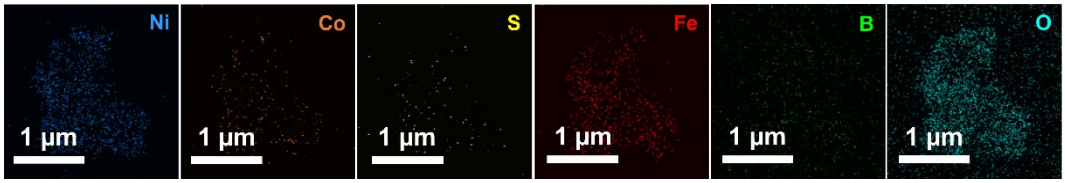

Fig. S16. The elemental mapping images of FeBO/Co-Ni_3S_2 after the OER stability test.

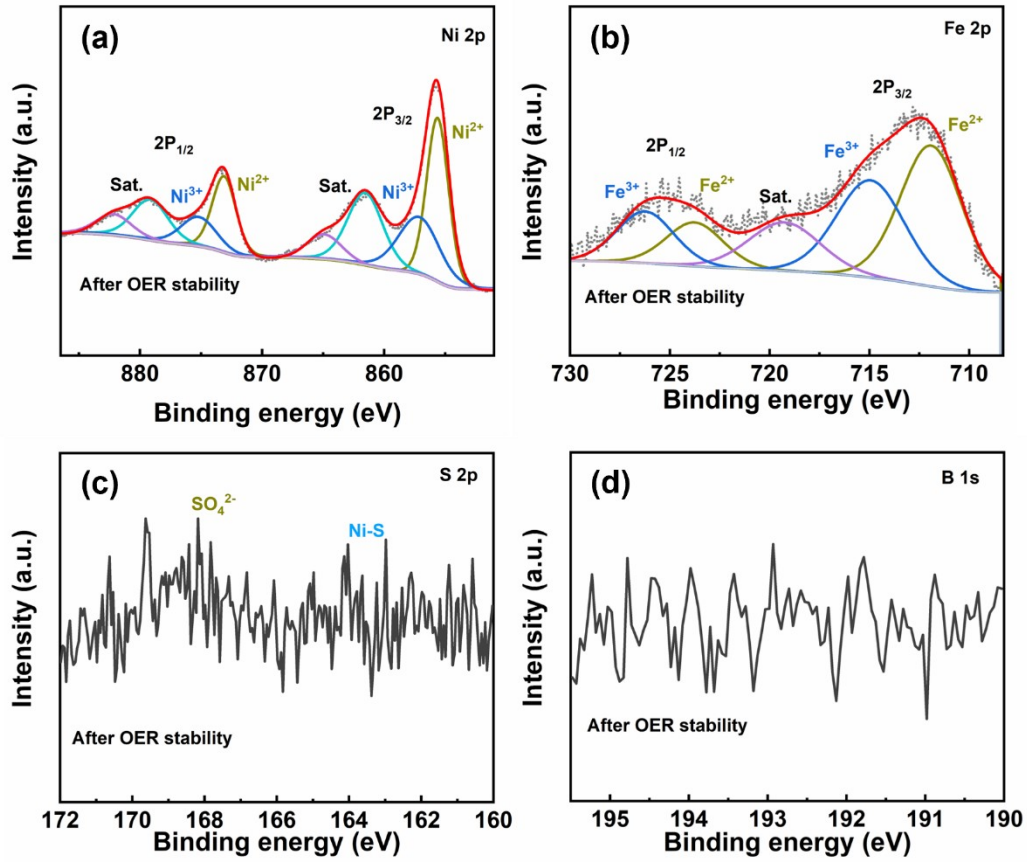

Fig. S17. Fig. XPS spectrum of FeBO/Co-Ni_3S_2 before and after stability test, (a) Ni 2p; (b) Fe 2p; (c) S 2p; and (d) B 1s.

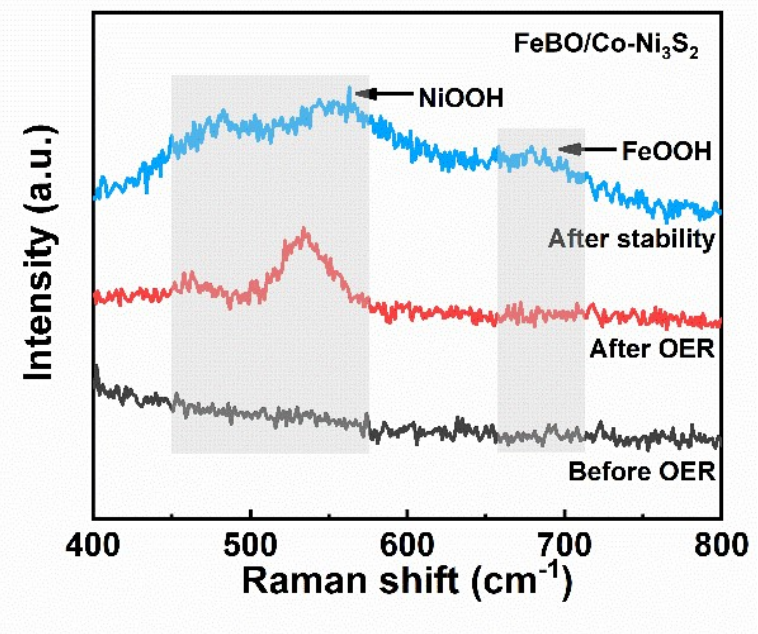

Fig. S18. Comparison of Raman spectra of FeBO/Co-Ni_3S_2 before, after OER, and after stability.

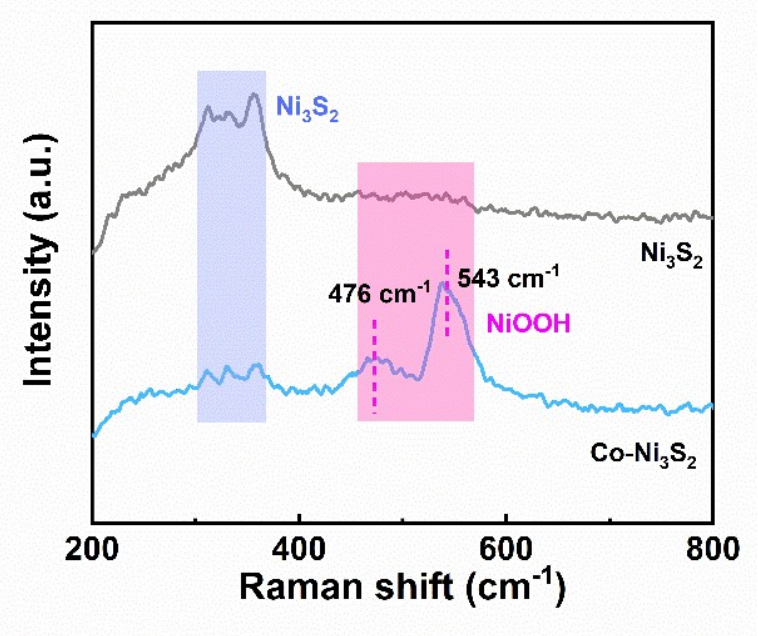

Fig. 19. Raman spectra of Co-Ni_3S_2, and Ni_3S_2 catalysts after OER test.

Table S3. Values of R_s and R_{ct} in the samples for MOR.

Sample	**R_s (Ω)**	**R_{ct} (Ω)**
FeBO/Co-Ni_3S_2	0.334	0.047
FeBO	0.334	1.28
Co-Ni_3S_2	0.385	0.874
Ni_3S_2	0.509	0.245

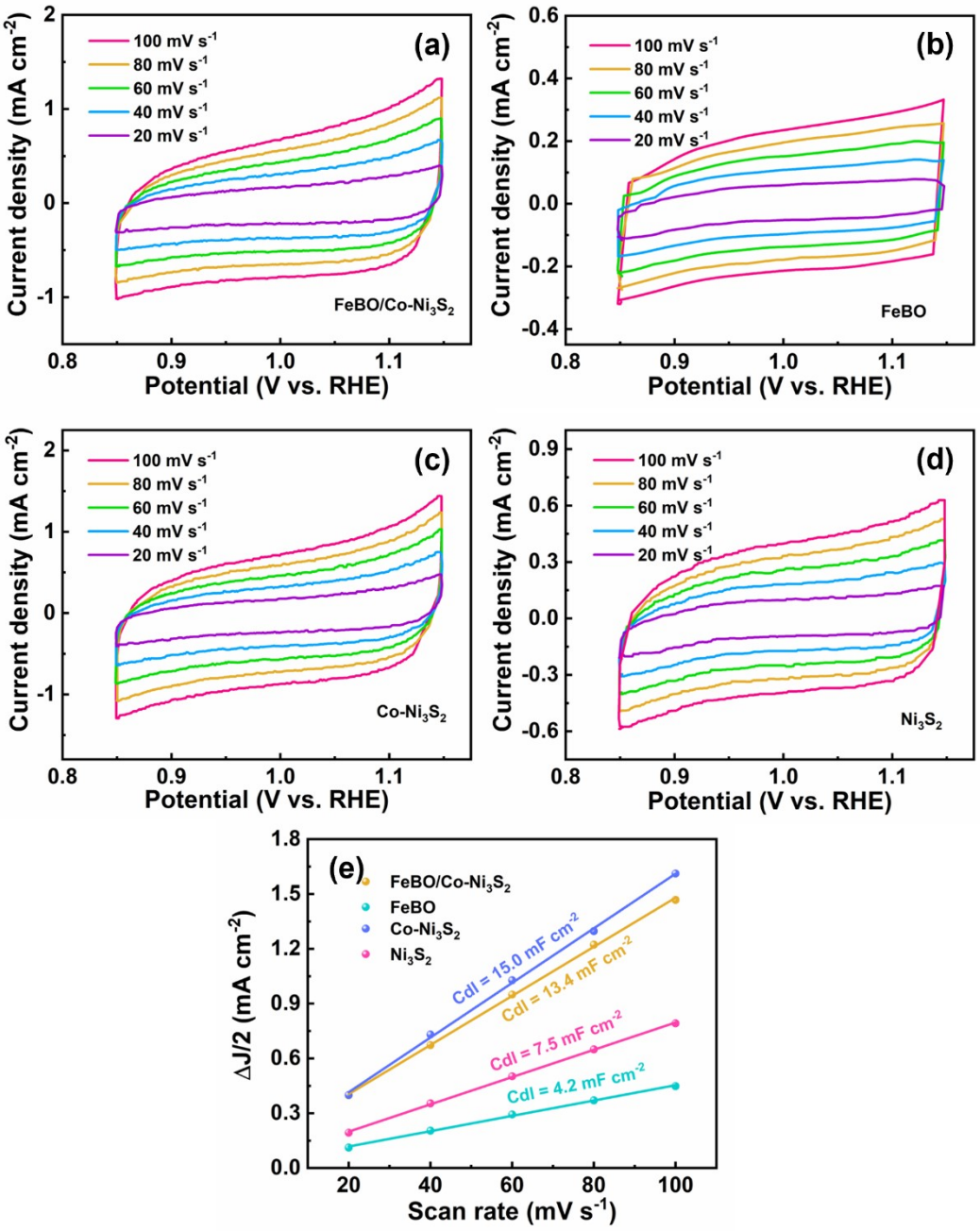

Fig. S20. CV curves of (a) FeBO/Co-Ni_3S_2, (b) FeBO, (c) Co-Ni_3S_2, and (d) Ni_3S_2 at different scan rates for MOR testing. (e) C_{dl} values.

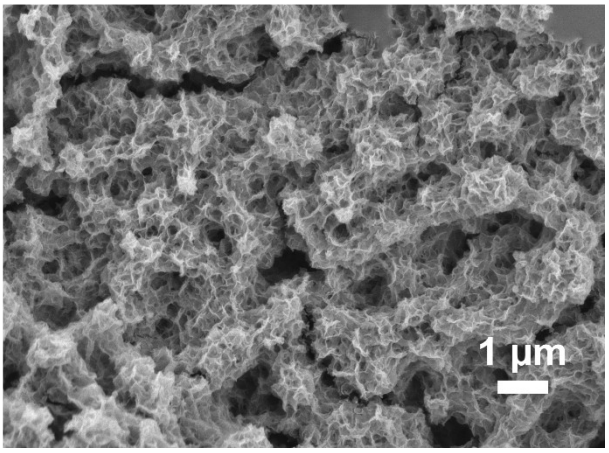

Fig. S21. The FE-SEM image of FeBO/Co-Ni_3S_2 after the MOR stability test.

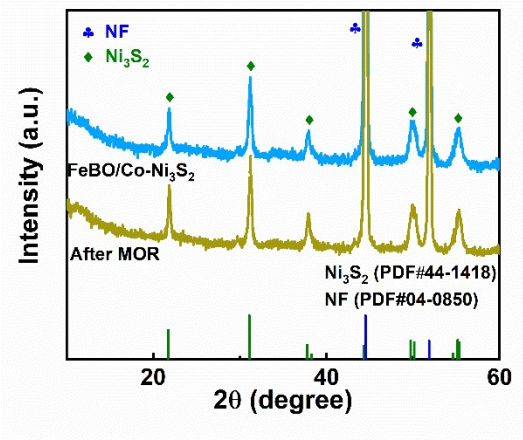

Fig. S22. The XRD image of FeBO/Co-Ni_3S_2 after the MOR stability test.

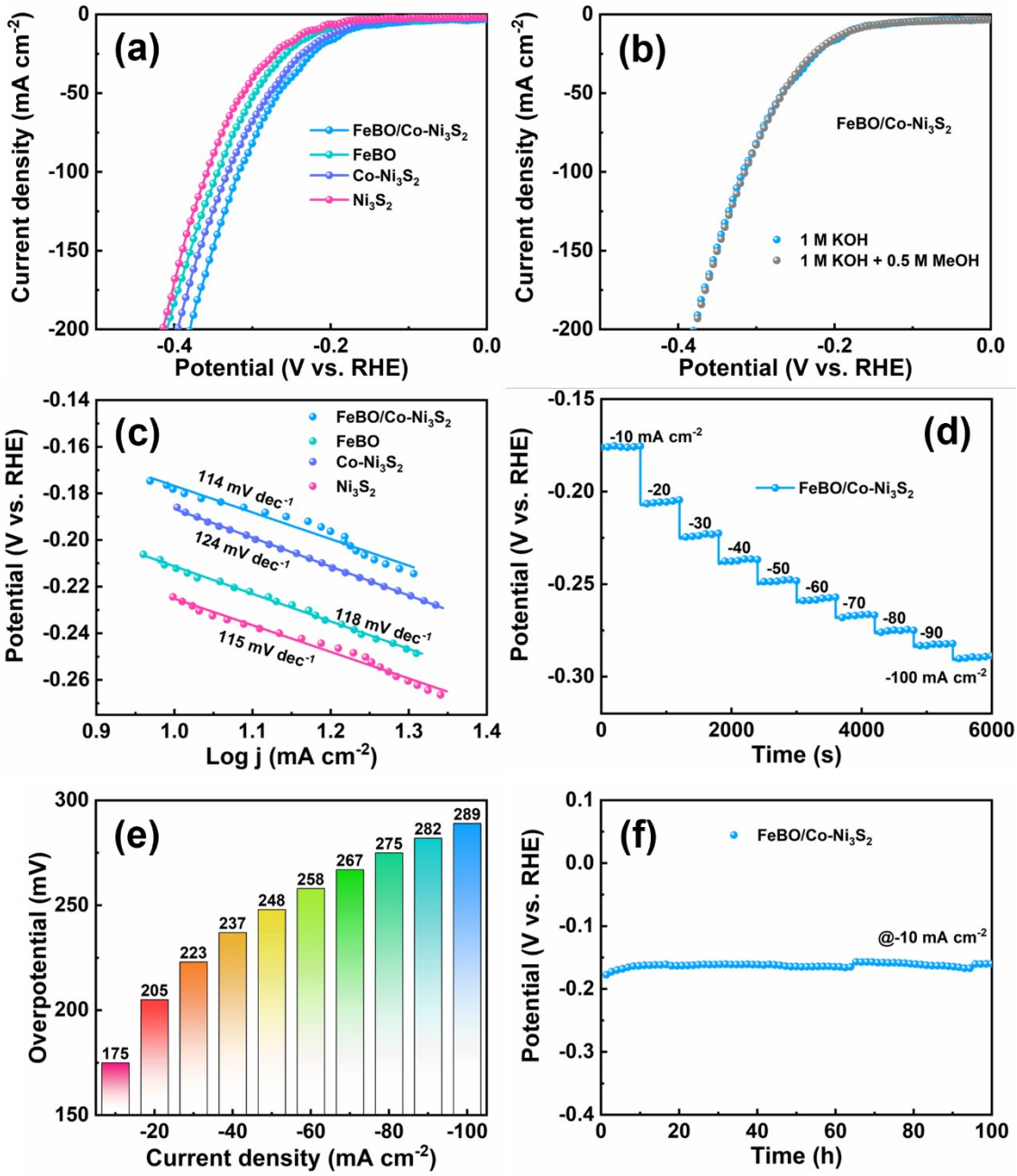

Fig. S23. (a) The LSV curves for the HER of various catalysts; (b) HER polarization plots of FeBO/Co-Ni_3S_2 in 1 M KOH electrolyte with and without 0.5 M methanol; (c) Tafel slopes for HER; (d) multi-current process of FeBO/Co-Ni_3S_2 and (e) corresponding overpotentials; (f) Long-term stability testing of HER.

Table S4. Comparison of the water and methanol electrolysis performance of FeBO/Co-Ni_3S_2 with previous.

Catalyst	**Voltage (V) @ j ($mAcm^{-2}$)**		**Stability (h) @10 j ($mAcm^{-2}$)**		**Ref.**
	OWS	OMS	OWS	OMS	
FeBO/Co-Ni_3S_2	**1.58 (η_{10}) 1.86 (η_{100})**	**1.44 (η_{10}) 1.67 (η_{100})**	**100**	**25**	**This work**
Pt–Ni_3S_2	1.886 (η_{100})	1.71 (η_{10})	-	36	[10]
Ni_3S_2/MoS_2	1.62 (η_{10})	-	100	-	[11]
Ni_3S_2@G	1.66 (η_{10})	-	30	-	[12]
3DG–Au-Ni_3S_2	1.63 (η_{10})	-	19	-	[13]
Ni_3S_2@Ni	1.61 (η_{10})	-	30	-	[14]
Ni-Co-S HPNA	1.62 (η_{10})	-	24	-	[15]
FeNi@FeNiB-700	1.65 (η_{10})	-	12	-	[16]
Fe_1Mn_1@BN-PCFs	1.622 (η_{10})	-	30	-	[17]
Co-S-INF	1.82 (η_{100})	1.70 (η_{100})	27	27	[18]
Co-Rh_2	-	1.545 (η_{10})	-	4	[19]
$NiTe_2$/Ni	1.77 (η_{10})	1.54 (η_{10})	12	12	[20]
$Co(OH)_2$@HOS/CP	1.631 (η_{10})	1.497 (η_{10})	-	20	[21]

The H_2 yield is calculated using the formula, H_2 yield rate = (V(experimental)/V(theoretical)) x 100%. The theoretical amount of H_2 released (V(theoretical)), is calculated using Faraday's law:

$$V_{Theo} = IRTt/PzF$$

V_{Theo} = Theoretical volume of evolved gas

I is working current density (I = 100 mA cm^{-2})

T is working temperature (T = 298 K), and 't' is time interval (t = 1200, 2400, and 3600 s)

R is the gas constant (R = 8.314459), and 'P' is the working pressure (P = 101.3 Kpa)

F is the Faraday's constant (F = 96485 C)

z is the number of electrons for generating 1 mol H_2 (z = 2)

The actual amount of H_2 produced during the electrolysis process was collected using a homemade H-type water electrolysis device in the laboratory and a water displacement method. Electrolysis conditions: The electrolysis was carried out in a two-electrode electrolytic cell with FeBO/Co-Ni_3S_2 electrodes and a controlled current density (100 mA cm^{-2}) for 1 h, where 1 M KOH and 1 M KOH + 0.5 M MeOH were used as electrolytes. The H_2 production results are visually represented in Fig. S24 and S25.

H_2 yield rate was calculated using the following equation:

$$H_2 \text{ yield rate} = Vg(\text{experimental})/Vg(\text{theoretical}) \times 100\%.$$

The H_2 yield rate of the two-electrode system is shown in Table S5.

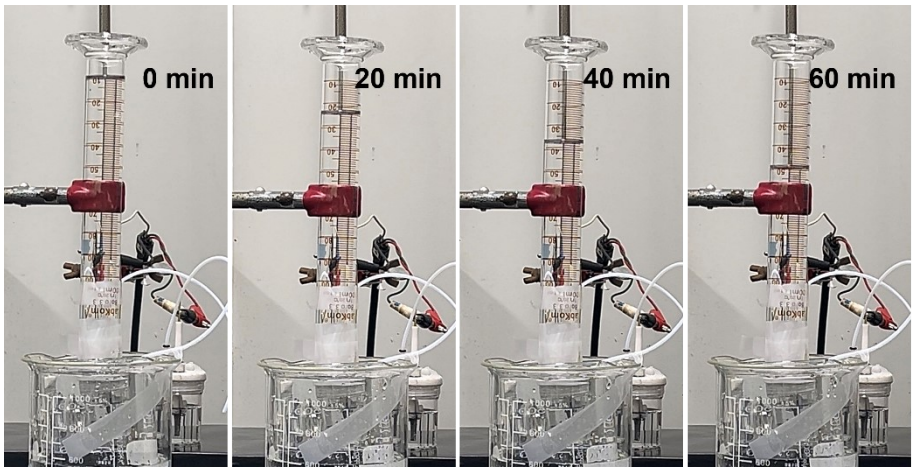

Fig. S24. The HER/OER dual-electrode system expands the drainage device during H_2 collection at different intervals.

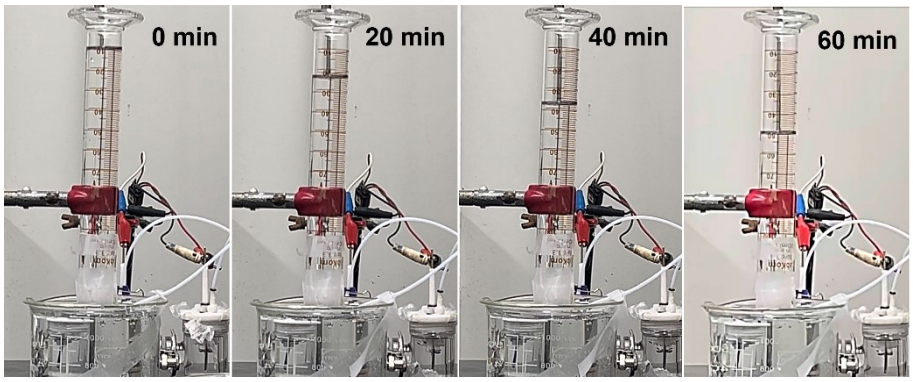

Fig. S25. The HER/MOR dual-electrode system expands the drainage device during H_2 collection at different intervals.

Table S5. The H_2 yield rate of the two-electrode systems.

System / Time	H_2 yield rate	
	HER/OER	HER/MOR
20 min	99%	95%
40 min	92%	92%
60 min	88%	89%
Average	93%	92%

References

1. G. Zhang, Y. S. Feng, W. T. Lu, D. He, C. Y. Wang, Y. K. Li, X. Y. Wang and F. F. Cao, *Acs Catalysis*, 2018, **8**, 5431-+.
2. J. Zhang, T. Wang, D. Pohl, B. Rellinghaus, R. H. Dong, S. H. Liu, X. D. Zhuang and X. L. Feng, *Angewandte Chemie-International Edition*, 2016, **55**, 6702-6707.
3. Y. Q. Yang, K. Zhang, H. L. Ling, X. Li, H. C. Chan, L. C. Yang and Q. S. Gao, *Acs Catalysis*, 2017, **7**, 2357-2366.
4. L. Y. Zeng, K. A. Sun, X. B. Wang, Y. Q. Liu, Y. Pan, Z. Liu, D. W. Cao, Y. Song, S. H. Liu and C. G. Liu, *Nano Energy*, 2018, **51**, 26-36.
5. H. Liu, J. N. Cheng, W. J. He, Y. Li, J. Mao, X. R. Zheng, C. Chen, C. X. Cui and Q. Y. Hao, *Applied Catalysis B-Environment and Energy*, 2022, **304**, 120935.
6. C. Z. Wang, X. D. Shao, J. Pan, J. G. Hu and X. Y. Xu, *Applied Catalysis B-Environmental*, 2020, **268**, 118435.
7. S. F. Zhou, H. W. He, J. Li, Z. H. Ye, Z. Liu, J. W. Shi, Y. Hu and W. W. Cai, *Advanced Functional Materials*, 2023, **34**, 2313770.
8. A. Kafle, D. Gupta and T. C. Nagaiah, *Electrochimica Acta*, 2023, **441**, 141779.
9. D. M. Shao, P. W. Li, R. Z. Zhang, C. H. Zhao, D. Q. Wang and C. J. Zhao, *International Journal of Hydrogen Energy*, 2019, **44**, 2664-2674.
10. Q. Q. Zhao, B. Zhao, X. Long, R. F. Feng, M. Shakouri, A. Paterson, Q. F. Xiao, Y. Zhang, X. Z. Fu and J. L. Luo, *Nano-Micro Letters*, 2024, **16**, 80.
11. S. Kim, K. Min, H. Kim, R. Yoo, S. E. Shim, D. Lim and S. H. Baeck, *International Journal of Hydrogen Energy*, 2022, **47**, 8165-8176.

12. J. Yu, Y. Du, Q. Q. Li, L. Zhen, V. P. Dravid, J. S. Wu and C. Y. Xu, *Applied Surface Science*, 2019, **465**, 772-779.

13. H. C. Tsai, B. Vedhanarayanan and T. W. Lin, *Acs Applied Energy Materials*, 2019, **2**, 3708-3716.

14. B. X. Wu, H. Qian, Z. W. Nie, Z. P. Luo, Z. X. Wu, P. Liu, H. He, J. H. Wu, S. G. Chen and F. F. Zhang, *Journal of Energy Chemistry*, 2020, **46**, 178-186.

15. W. X. Chen, Y. W. Zhang, G. L. Chen, R. Huang, Y. J. Wu, Y. M. Zhou, Y. J. Hu and K. Ostrikov, *Journal of Colloid and Interface Science*, 2020, **560**, 426-435.

16. H. F. Yuan, S. M. Wang, X. D. Gu, B. Tang, J. P. Li and X. G. Wang, *Journal of Materials Chemistry A*, 2019, **7**, 19554-19564.

17. Z. Liu, F. Guo, L. Cheng, X. J. Bo, T. T. Liu and M. A. Li, *Journal of Colloid and Interface Science*, 2023, **629**, 179-192.

18. J. X. Dang, G. M. Chen, B. E. Yuan, F. Y. Liu, Q. Wang, F. Wang, H. Miao and J. L. Yuan, *Nanoscale*, 2024, **16**, 4710-4723.

19. Y. Guo, X. B. Yang, X. C. Liu, X. L. Tong and N. J. Yang, *Advanced Functional Materials*, 2023, **33**, 2209134.

20. S. Anantharaj, M. C. Li, R. Arulraj, K. Eswaran, C. M. S. Fidha, R. Murugesan, A. Maruthapillai and S. Noda, *Chemical Communications*, 2023, **59**, 12755-12758.

21. K. Xiang, D. Wu, X. H. Deng, M. Li, S. Y. Chen, P. P. Hao, X. F. Guo, J. L. Luo and X. Z. Fu, *Advanced Functional Materials*, 2020, **30**, 1909610.